DESY 95-043

arXiv:hep-ex/9503011 17 Mar 1995

DESY-95-043, hep-ph/9503011

Photon Structure as seen at HERA *

J. M. Butterworth
Dept. of Physics, Penn State University,
University Park, PA 16802, USA.

Representing the ZEUS and H1 collaborations

Abstract

At HERA, the electron-proton collider at DESY, Hamburg, the large flux of almost on-shell photons accompanying the lepton beam is being used to shed new light on the structure of the photon. Recent results are reviewed and discussed, with emphasis on those aspects of the photon's nature which should be understandable using perturbative QCD.

*Presented at the 3rd Workshop on TRISTAN Physics at High Luminosities, November 16-18, 1994, KEK, Tsukuba, Japan

1 Introduction

At DESY, Hamburg, 820 GeV protons collide with 27 GeV electrons (or positrons) in HERA. Two general purpose detectors, H1 [1] and ZEUS [2], are positioned at opposing interaction points on the accelerator ring. The high flux of almost on-shell photons which accompanies the lepton beam provides a unique opportunity to study the nature of the photon and its interactions.

Collisions take place between protons and almost on-shell photons (with a negative mass squared in the range $10^{-10} < Q^2 < 4$ GeV^2), at γp centre-of-mass energies ($W_{\gamma p}$) up to 300 GeV, an order of magnitude greater than previously available. HERA does not, of course, measure the structure function F_2^γ, as this is defined in terms of the scattering of electrons off photons. However, studies of jet production in γp interactions provide information about the photon structure down to momentum fractions as low as 5×10^{-2}, and because the photon is being probed by partons from the proton, there is a high sensitivity to the distribution of gluons in the photon.

The presence of a 'hard' energy scale (usually from the high transverse energy (E_T^{jet}) of the jets) means that perturbative QCD calculations of event properties can be confronted with experiment. Examples of leading order (LO) QCD diagrams for photoproduction at HERA are shown in figure 1. At this order, two processes are responsible for jet production. The photon may interact directly with a parton in the proton (figure 1a), or it may first fluctuate into an hadronic state (figure 1b). In the first case, known as the direct contribution, the fraction of the photon momentum (x_γ) participating in the hard process is one. The final state consists of two jets, the proton remnant and the scattered electron. In the second case, known as the resolved contribution, the photon acts as a source of partons, which then scatter off partons in the proton, and x_γ is less than one. The final state in this case includes a photon remnant, continuing in the original photon direction, in addition to two jets, the proton remnant and the scattered electron. Direct photon events do not involve the photon structure, but can probe the parton distributions in the proton down to $x_p \approx 10^{-3}$, where x_p is the fraction of the proton's momentum entering into the hard process. This process is directly sensitive to the gluon distribution in the proton, and complements indirect extractions [3] using the measurement of F_2 in deep inelastic scattering (DIS).

Seen from a perspective of understanding and testing QCD, photoproduction at HERA provides information about quark and gluon interactions in the γp system over a broad range of kinematic variables, information that is complementary to that obtained from DIS, either in ep events at HERA or in $e\gamma$ events at TRISTAN and LEP.

Both the ZEUS and H1 detectors have high resolution calorimeters and tracking chambers.

Jets have been measured in the pseudorapidity[1] region $-1 > \eta > 2.5$ and with E_T^{jet} in the range $6 < E_T^{jet} < 37$ GeV.

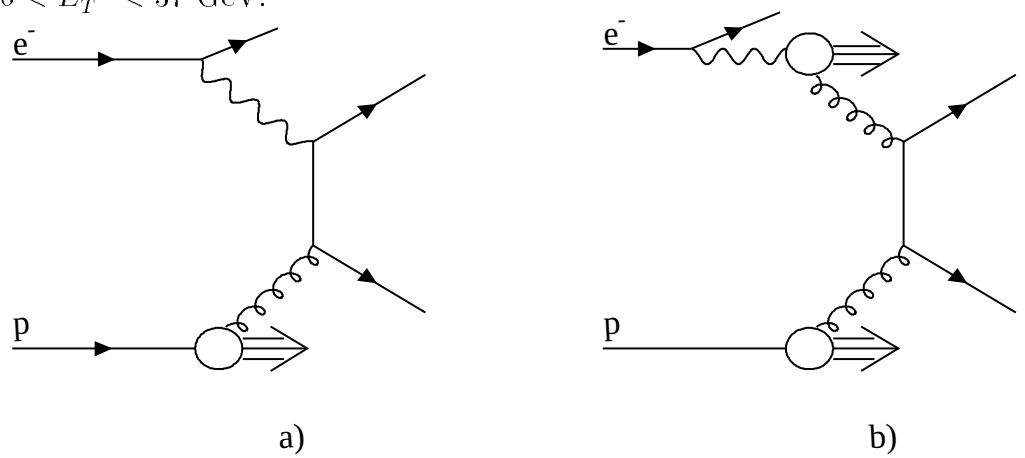

Figure 1: Examples of leading order diagrams for a) direct and b) resolved photoproduction.

2 Untangling the Subprocesses

Because of the large cross sections involved, photoproduction physics provided interesting results very soon after HERA began colliding the beams. At that time, evidence for 'hard' interactions in the resolved photon process had just been observed for the first time, by the AMY collaboration [4]. Both the ZEUS and H1 collaborations rapidly provided confirmation of hard scattering from partons inside the resolved photon, this time in γp events [5]. Jet production was seen, and energy flow in the rear (electron) direction provided clear evidence for the presence of a photon remnant.

In events with two (or more) jets, the parton kinematics of photoproduction events can be reconstructed. In particular, the momentum fractions of the photon and proton can be measured. For two-to-two parton scattering in LO QCD, energy and momentum conservation give the fraction of the photon energy involved in the hard scatter as

$$x_\gamma^{LO} = \frac{\sum_{partons} E_T^{parton} e^{-\eta^{parton}}}{2yE_e}, \qquad (1)$$

[1]The z axis is defined to lie along the proton direction, and $\eta = -\ln(\tan\frac{\theta}{2})$ where θ is the angle between the jet and the z axis.

$$x_p^{LO} = \frac{\sum_{partons} E_T^{parton} e^{\eta^{parton}}}{2E_p}, \tag{2}$$

where yE_e is the initial photon energy, E_p is the proton energy, and the sum is over the two final state partons. For direct photon events, $x_\gamma^{LO} = 1$. For those events in which two jets are observed in the detector, it is possible to estimate the fraction of the photon momentum which participates in the hard process by replacing the sum over partons in equation (1) with a sum over jets. It is then possible to make an explicit definition of the observable x_γ,

$$x_\gamma^{OBS} = \frac{\sum_{jets} E_T^{jet} e^{-\eta^{jet}}}{2yE_e}, \tag{3}$$

where now the sum runs over the two jets of highest E_T^{jet}. An analogous definition can be made for the proton momentum fraction. In the x_γ^{OBS} distribution thus obtained, the LO direct and resolved processes populate different regions, with the direct processes concentrated at high values of x_γ^{OBS}. The peak arising from the direct contribution will not necessarily lie exactly at $x_\gamma^{OBS} = 1$, due to higher order effects and/or hadronisation, but will still correspond to the kinematic region where most or all of the energy of the photon participates in the hard subprocess. This treatment avoids possible confusion arising due to the fact the simple separation between resolved and direct processes is only possible at LO in QCD and x_γ^{LO} becomes ambiguous even at next-to-leading order (NLO).

The x_γ^{OBS} and x_p^{OBS} distributions (not corrected for detector effects, and therfore called x^{meas}) measured by the ZEUS collaboration using 1992 data [6] are shown in figure 2. The x_γ^{OBS} distribution (figure 2b) rises at both low and high values. The Monte Carlo simulations of the resolved and direct processes (which also include detector effects) shown in the same figure, have very different characteristics. The resolved processes show a rise towards low x_γ^{OBS}, as observed in the data, but cannot account for the rise at high x_γ^{OBS}. The direct processes predict a sharp rise towards high x_γ^{OBS} as observed in the data and only a small number of events for $x_\gamma^{OBS} < 0.7$. The conclusion is that the peak at the high end of the x_γ^{OBS} distribution results from direct processes.

3 Jet Cross Sections

The results presented in the previous section show good qualitative agreement between the data and QCD expectations, in the sense that the expected production mechanisms and event topologies are observed. However, signs of discrepancies are already seen. In particular, when the transverse energy flow around the jets is studied, more energy was seen in the data in the forward (proton)

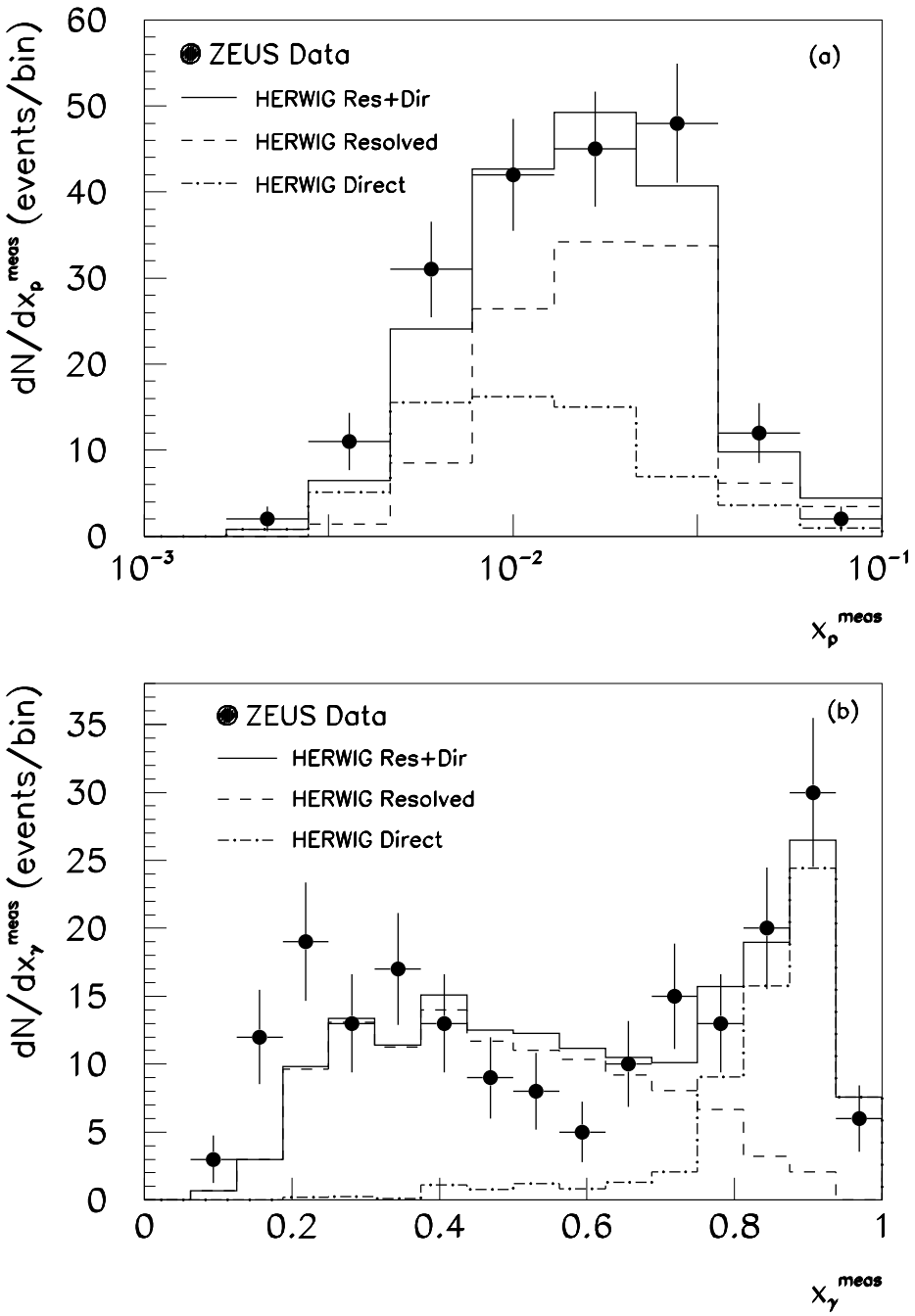

Figure 2: Kinematic distributions for events with two or more jets. (a) x_p^{meas} (*i.e.* uncorrected x_p^{OBS}) distribution for the final sample. (b) x_γ^{meas} (*i.e.* uncorrected x_γ^{OBS}) distribution for the final sample.

region than was expected from Monte Carlo simulations [7]. In addition, in figure 2 there is an excess of low x_γ^{OBS} events in the data over the simulation. In order to obtain quantitative information from photoproduction processes, clearly defined cross sections must be measured and compared with theoretical calculations. I concentrate here on jet cross sections, although much information can be also be obtained from measurements of charged particle spectra [8].

3.1 Inclusive Jet Cross Sections

Inclusive jet cross sections provide a good test of perturbative QCD, and have been measured by both the H1 [7] and ZEUS [9] collaborations. At both experiments, jet finding is performed using a cone algorithm [10]. The cone radius of the jet finding algorithm is typically defined such that $R = \sqrt{\Delta\eta_{cell}^2 + \Delta\phi_{cell}^2} = 1$, although other values could also be used in the future. The algorithm searches in pseudorapidity-azimuth (η_{cell}-ϕ_{cell}) space for the cone containing the highest summed E_T.

H1 use the electron calorimeter of their luminosity monitor [7] to measure the energy of the low angle scattered electron in the range $0.25 < y < 0.7$, where $y = E_\gamma/E_e$, the fraction of the initial electron energy (E_e) carried by the almost real photon with energy E_γ. The corresponding range of photon virtualities is approximately 10^{-8} GeV^2 $< Q^2 <$ 0.01. For jet studies at ZEUS, photoproduction events are usually defined by demanding that the electron is scattered at small angles and does not emerge from the beam pipe with the central ZEUS detector. This requirement corresponds approximately to a cut of $Q^2 < 4$ GeV^2. The range of y values used by ZEUS is $0.2 < y < 0.85$.

The inclusive jet cross cross section $d\sigma/d\eta$ measured by the ZEUS collaboration is shown in figure 3. Also shown are the cross sections calculated by the PYTHIA [11] Monte Carlo model (including the effects of hadronisation and parton showering). The model with both the photon parton distribution sets shown describes the data well, with only a small discrepancy in the foward (high η) region for the low E_T^{jet} cross section. The inclusive jet cross section $d\sigma/dE_T^{jet}$ is shown in figure 4, for two different ranges of η^{jet}, one of which includes the forward region and the other of which excludes it.

Given the failure of the Monte Carlo models used here to describe the energy flow in the forward region shown in ref. [7]) it is not surprising that the cross sections do not completely agree in the forward region at low E_T^{jet}. At higher E_T^{jet} the uncertainties arising from hadronisation can be expected to become less significant, and any test of QCD *via* such comparisons becomes less ambiguous. NLO calculations of these processes are already becoming available [12].

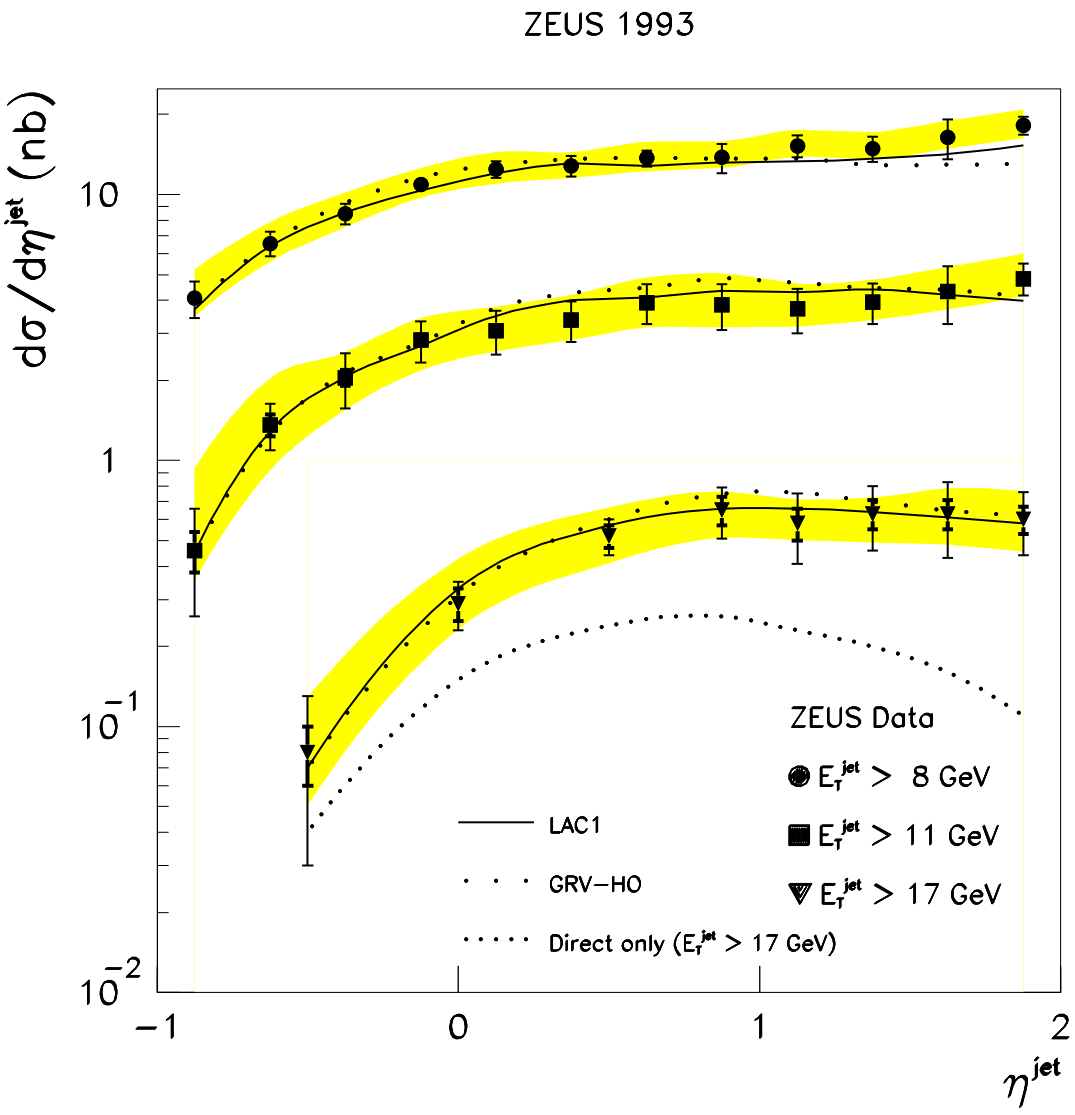

Figure 3: Differential ep cross section $d\sigma/d\eta$ for inclusive jet production, integrated over E_T^{jet} from three different thresholds ($E_T^{jet} > 8, 11$ and 17 GeV) in the kinematic region defined by $Q^2 \leq 4$ GeV^2 and $0.2 > y > 0.85$. PYTHIA calculations are shown for comparison.

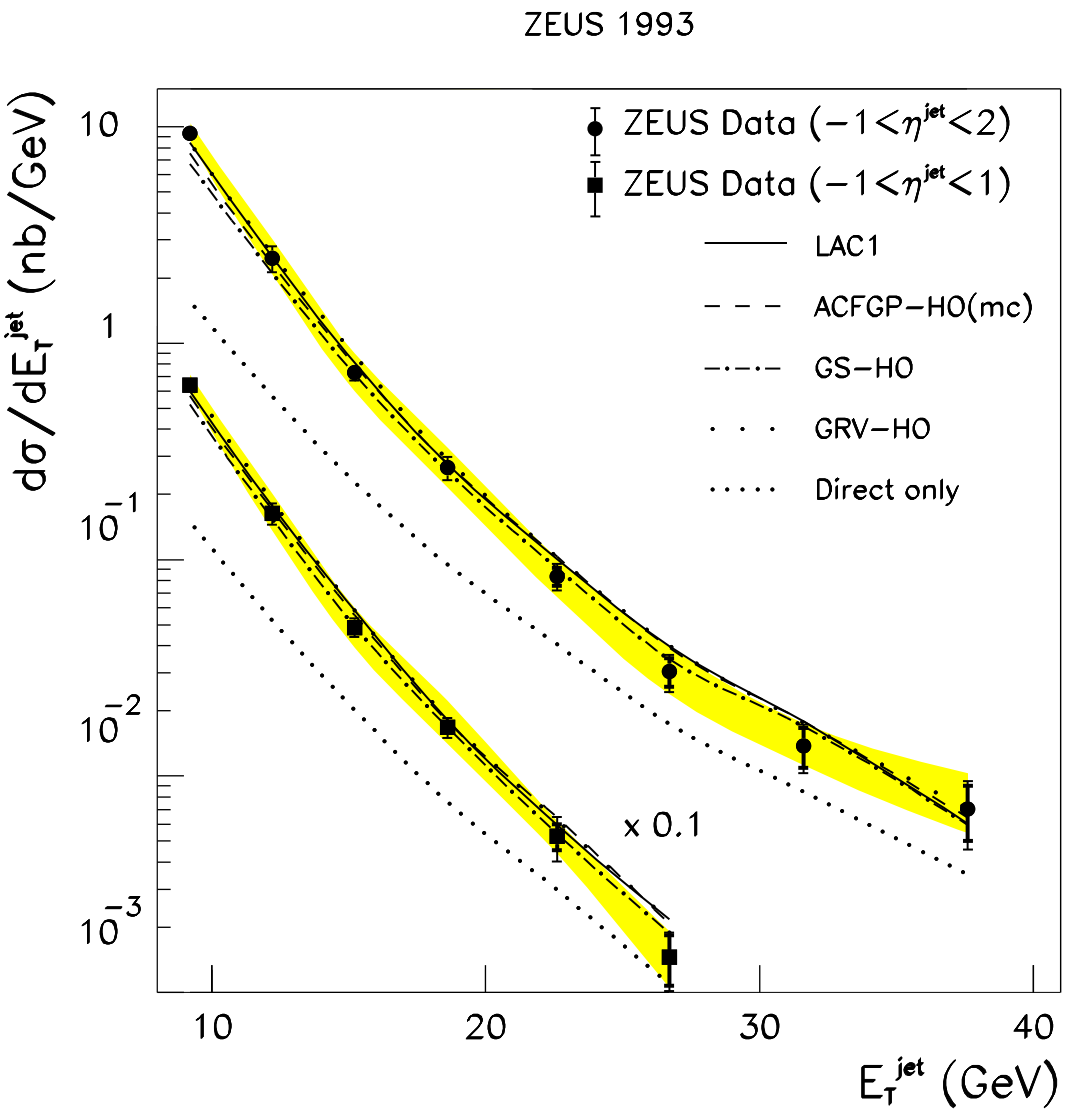

Figure 4: Differential ep cross section $d\sigma/dE_T^{jet}$ for inclusive jet production, integrated over two η^{jet} ranges ($-1 < \eta^{jet} < 2$ and $-1 < \eta^{jet} < 1$) in the kinematic region defined by $Q^2 \leq 4$ GeV^2 and $0.2 > y > 0.85$. PYTHIA calculations are shown for comparison. For the latter η^{jet} range, both Monte Carlo curves and data have been multiplied by 0.1.

3.2 Dijet Cross Sections

Although inclusive jet cross sections have the advantage of calculational simplicity, there are advantages in measuring dijet cross sections. In this case, reconstruction of the kinematics of the hard scatter becomes possible, in particular of x_γ^{OBS} and x_p^{OBS}. By making kinematic cuts it is possible to untangle some of the many unknowns in the photoproduction process, in particular the dependence upon the parton distributions in the proton and photon.

The ZEUS collaboration has measured the differential cross section $d\sigma/d\bar{\eta}$ for dijet photoproduction [13]
($ep \rightarrow e\gamma\, p \rightarrow e\, X + 2$ jets) in the y interval $0.2 < y < 0.8$, for events with at least two jets of $E_T^{jet} > 6$ GeV, and a difference in the pseudorapidities of the two jets of $|\Delta\eta| < 0.5$. The variable $\bar{\eta} = \frac{1}{2}(\eta_1 + \eta_2)$ is the average pseudorapidity of the two jets of highest transverse energy. This cross section is measured separately for resolved and direct photon events, as defined by a cut on x_γ^{OBS} at 0.75, with the low x_γ^{OBS} events identified with resolved photoproduction and the high x_γ^{OBS} events identified as direct photoproduction. The expression for x_γ^{OBS} (equation 3) can be rewritten in terms of $|\Delta\eta|$ and $\bar{\eta}$, assuming the jets to have equal transverse energy, to obtain

$$x_\gamma^{OBS} = \frac{E_T^{jet} e^{-\bar{\eta}}}{yE_e} \cosh\frac{\Delta\eta}{2}. \tag{4}$$

A similar expression can be written for the proton,

$$x_p^{OBS} = \frac{E_T^{jet} e^{\bar{\eta}}}{E_p} \cosh\frac{\Delta\eta}{2}. \tag{5}$$

Constraining the jets to be at almost equal pseudorapidities, with the cuts on $|\Delta\eta|$, means that the hyperbolic cosine term takes its minimum value of unity. Thus the minimum available x values are probed for a given E_T^{jet} and $\bar{\eta}$, and there is a strong correlation between $\bar{\eta}$ and x_p^{OBS} in the direct cross section and between $\bar{\eta}$ and yx_γ^{OBS} in the resolved cross section [14].

The direct cross section is shown in figure 5a, compared to leading order QCD calculations using various different parton distribution sets for the proton. The parton distribution sets used are the GRV LO [15], CTEQ2M [16], MRSA [17] and MRSD$'_0$ [18] parton distribution sets for the proton. The shape of the direct cross section differs from that of the LO QCD calculations. However, several effects (apart from the choice of parton distribution set) influence the comparison between data and theory. QCD calculations are only available at LO, and higher order corrections may be large. Also, due to the fact that we are probing low x partons in the proton, the standard approximation that the incoming partons are collinear and on-shell may be invalid [20]. Finally, non-perturbative 'hadronisation' effects can be expected to be significant. Considering these uncertainties the agreement with the theory is fairly good.

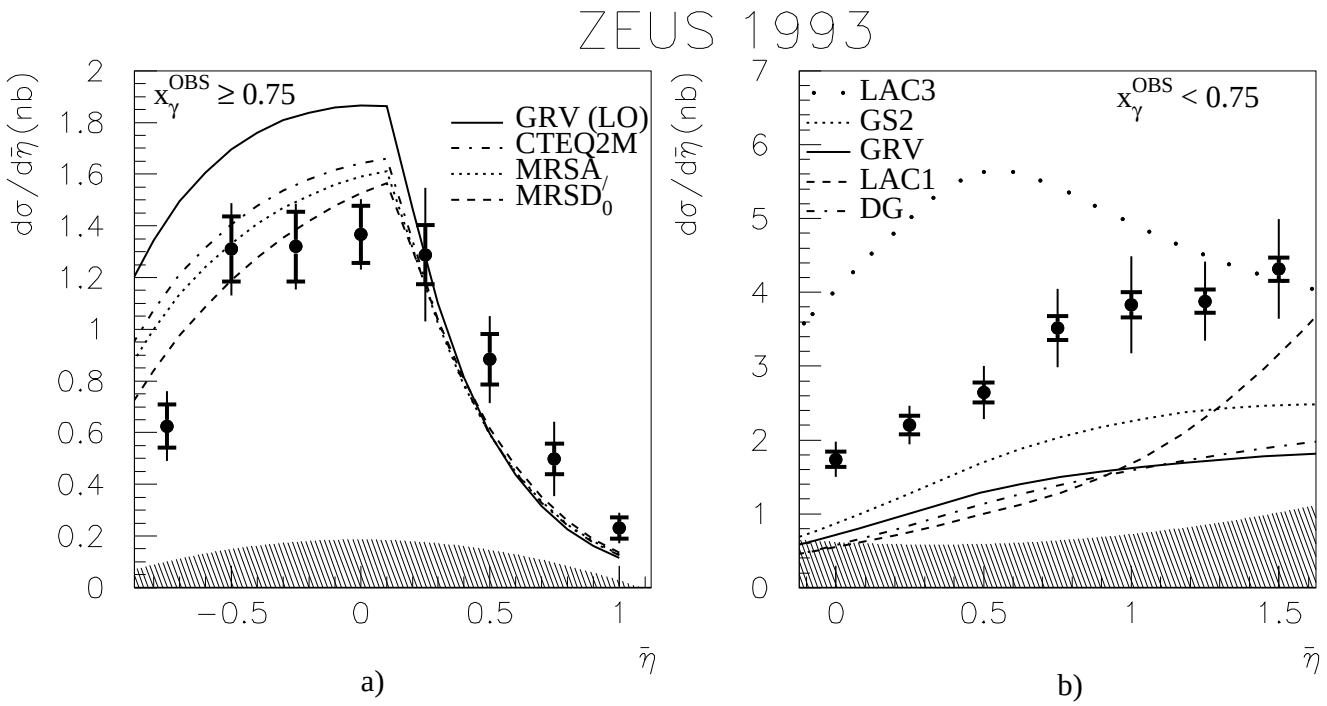

Figure 5: $d\sigma/d\bar{\eta}$ for $ep \to eX + 2$ jets, $|\Delta\eta| < 0.5, E_T^{jet} > 6$ GeV, $0.2 < y < 0.8, Q^2 <$ 4 GeV^2, a) $x_\gamma^{OBS} \geq 0.75$, b) $x_\gamma^{OBS} \geq 0.75$, The solid circles are corrected ZEUS data. The inner error bars indicate the statistical errors, the outer error bars show the systematic uncertainty excluding the the correlated uncertainty from measurement of energy in the calorimeter and the integrated luminosity, which are show as a shaded band. In a) the data are compared to LO QCD calculations using several parton distribution sets for the proton and the GS2 set for the photon. In b) the data are compared to LO QCD calculations using the LAC3, GS2, GRV, LAC1 and DG parton distribution for the photon. The proton parton distribution set used is the MRSA set.

Figure 5b shows the measured cross section $d\sigma/d\bar{\eta}$ for resolved photoproduction. The LO cross sections, shown for comparison, are calculated using different photon parton distribution sets and the MRSA [17] set for the proton. The theoretical sensitivity to the parton distributions in the proton is small (not shown), with the variations between curves calculated using different parton distribution sets being much less than the estimated errors on the measured cross section. The DG [21], GRV [15] and GS2 [22] parton distribution sets reproduce the shape of the cross section well and can be brought into agreement with the data by applying a multiplicative factor of around 2. Factors of this size may reasonably be expected to come from NLO calculations [12]. The LO calculations using the LAC1 and LAC3 [23] parton distribution sets cannot be brought into agreement with the data by a constant normalization factor.

4 Photon Structure

The Monte Carlo simulations discussed so far attempt to describe photoproduction by a hard parton-parton subprocess coupled with parton distributions in the proton and photon and parton shower and hadronisation models. No allowance is made for the possibility of further interactions (other than a single parton-parton scattering) taking place in a γp event. In obtaining the results shown, the simulations are only used to correct for detector acceptance and smearing. The effects of the discrepancies between the Monte Carlo simulations and the data on the measurement of the cross sections are estimated and included in the systematic errors. Thus the cross sections can be presented as measurements of observed jet cross sections with confidence. However, this confidence evaporates when we come to interpret the cross sections in terms of parton distributions. If there are unknown other processes contributing to the energy flow in the event, they will distort the correlation between 'parton' kinematic variables in the model and jet variables in the data.

As an example of this, figure 6 shows the uncorrected transverse energy flow per jet $1/N dE_T/d\delta\eta$ around the jet axis for events entering the two dijet cross sections of figure 5. For the events with $x_\gamma^{cal} \geq 0.75$ (direct events, figure 5a and figure 6a), both the HERWIG [24] and PYTHIA simulations reproduce the data distribution well. The same distribution is shown in figure 6b for events with $x_\gamma^{cal} < 0.75$ (resolved). In this case both simulations fail to describe the pedestal in the energy flow in the forward region, as was also observed (for inclusive jets without an x_γ^{OBS} cut) in references [7] and [9]. Thus when interpreting the cross section in figure 5b in terms of parton distributions, it is difficult to estimate what the effects of hadronisation and parton showering might be on the shapes of the curves, since the jet pedestal energies are not well described in the Monte Carlo. Therefore no parton distribution set (with the exception of LAC3) can be confidently excluded at this stage.

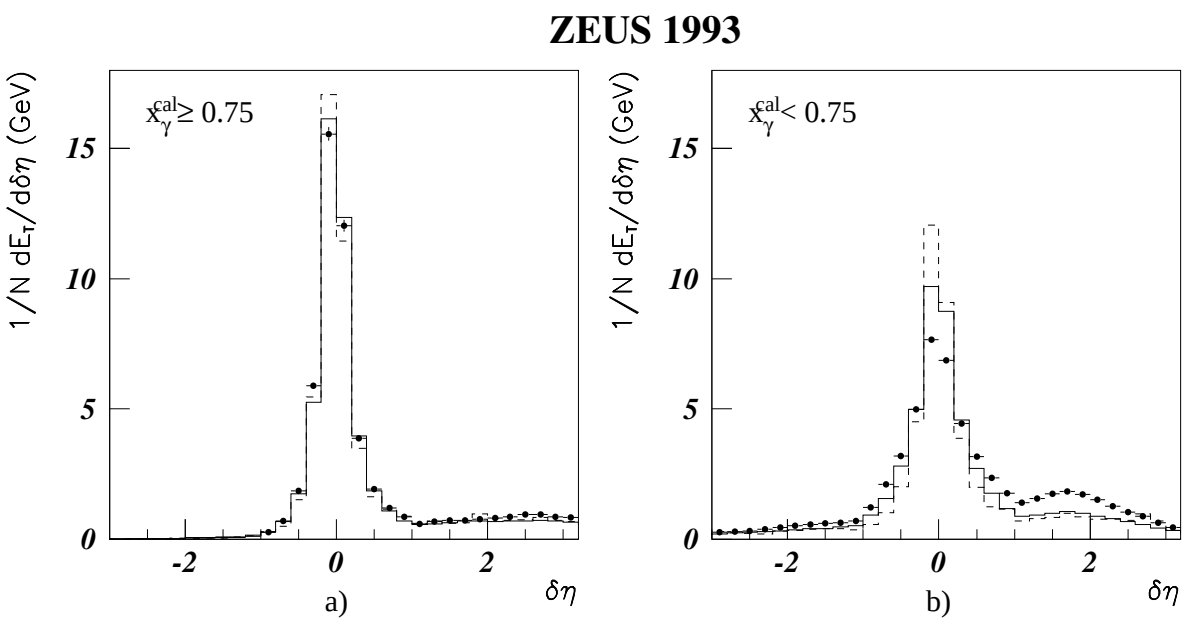

Figure 6: Figures a) and b) show the uncorrected transvserse energy flow $dE_T/d\delta\eta$ around the jet axis, for cells within one radian in ϕ of the jet axis, for a) direct and b) resolved events. The solid (dashed) line represents the distribution from PYTHIA (HERWIG).

4.1 Multiple Interactions

One candidate for improving the agreement between the Monte Carlo models and the data is to allow for the possiblity of more than one hard interaction per γp event [25]. This can happen because the parton densities probed at HERA are sufficiently large that even from a naive probabilistic point of view, the chance of more than one hard scatter in a γp interaction becomes significant. Models of this nature are usually called 'eikonal' models and are also used to regularise the strong growth exhibited in minijet calcuations of the γp cross section [26]. It has been demonstrated by H1 [27] that including some form of multiple interaction model can bring the Monte Carlo simulation into significantly better agreement with the data. As multiple interactions in this type of scenario are generated by the density of partons in the photon, they are expected to be absent in the direct process, where the photon parton distributions play no part. Returning to the jet profiles in the resolved and direct samples isolated by ZEUS in reference [13] (figure 6) the fact that the forward energy excess is not observed in the direct (high x_γ^{OBS}) events lends support to the idea that multiple hard interactions are a reality.

4.2 Parton Distributions

It is possible to use the PYTHIA multiple interaction model, together with an additional 'underlying' jet pedestal energy and the usual parton showering and hadronisation models, to obtain a good description of the energy flow around the jets [27]. Within this model, there then exists a particular correlation between the LO, generated partons and the observable jets. In the absence (so far) of better theoretical tools, it is interesting to assume that the Monte Carlo model represents the 'truth' as far as this correlation is concerned, and deduce what parton distribution is needed in the Monte Carlo simulation in order to successfully describe the observed jet rates. This procedure was carried out by H1, and the resulting x_γ^{LO} distribution is shown in figure 7.

Once this has been done, the fact that measurements of F_2^γ constrain the quark distributions in the photon in this kinematic region can be used to deduce what part of the parton density is attributable to gluons in this model. The result is shown in figure 8.

4.3 Remnant Structure

Most analyses of photoproduction events at HERA have implemented a cone algorithm to find jets. The cone algorithm uses a cone of fixed radius in pseudorapidity and azimuthal angle space and is well suited for high transverse energy jets at fairly central pseudorapidities. However, the photon remnant will mainly deposit energy at low angles relative

to the electron direction, over a large negative pseudorapidity range, and a clustering algorithm is more appropriate. ZEUS have used the k_T jet clustering algorithm in the laboratory frame [28, 29] to isolate and study this photon remnant [30].

This algorithm finds jets by calculating a quantity k_T for each calorimeter cell 'hit' with respect to all other hit cells. In the small angle approximation, k_T reduces to the transverse momentum squared of the lower energy cell with respect to the higher energy cell. The value of k_T for each pair of cells, or clusters, is calculated from the formula:

$$k_T = 2\min(E_n^2, E_m^2)(1 - \cos\theta_{nm}), \tag{6}$$

where E_n and E_m are the energies for cells n and m, and θ_{nm} is the angle between the two cells. When all of the k_T values of an event have been calculated, the two cells with the lowest k_T value are merged. This process is iterated, merging cells or clusters of cells, until the desired number of clusters remain. The proton remnant is included in the clustering procedure as a pseudo-particle which moves in the proton direction. For high transverse energy jets the K_t cluster finding algorithm gives results similar to those obtained with the usual cone algorithm.

The k_T algorithm was forced to find three energy clusters in each event, in addition to the cluster related to the proton remnant. The pseudorapidity $\eta^{cluster}$ distributions of the three clusters obtained with the k_T algorithm are shown in figure 9a-c, in order of decreasing transverse energy. The data (full circles) and MC (resolved and direct, histogram) are shown normalized in the region $\eta^{cluster} \leq 1.6$. While the first and second clusters are predominantly found in the $\eta^{cluster} \geq 0$ region, the third cluster has an accumulation in $\eta^{cluster} \leq 0$, *i.e.* the outgoing electron direction. The agreement between the data and the MC is reasonable for all three clusters except for the very forward region $\eta^{cluster} \geq 1.6$ where the discrepancies already noted in the forward energy flow can be expected to be significant. In particular the excess observed in figure 9c in the negative pseudorapidity region is well described by the Monte Carlo simulation including resolved and direct processes (full histogram). However the (LO) direct process does not contribute to this excess as shown by the dashed line in the figure; its distribution is rather flat as expected from the absence of photon remnants for this class of events. As a consequence, the third cluster in the negative pseudorapidity region can be identified with the photon remnant.

After requiring the first two clusters to be jets with $E_T^{jet} > 5$ GeV and pseudorapidity $\eta^{jet} < 1.6$, as in reference [6], the η distribution of the third cluster is shown in figure 1d. Compared with the MC expectations, the data show an excess toward higher η values corresponding to higher angles with respect to the electron direction. A cut of $\eta^{cluster_3} < -1$ was then applied to the third cluster. After these cuts, x_γ^{OBS} was found to peak at low values as expected for resolved processes.

The energy distribution for the third cluster is shown in figure 10a The solid histogram shows the Monte Carlo expectation which agrees reasonably with the data. The transverse momentum (with respect to the beam) distribution of the third cluster, shown in

figure 10b, peaks at 1 GeV with a tail extending to 6 GeV. The Monte Carlo expectation, shown in histogram, shows a lower average value. This is in qualitative agreement with the expectation is that the 'anomalous' component of resolved photoproduction, where the photon splits into a perturbatively calculable $q\bar{q}$ pair, should have a higher transverse energy remnant than the so-called Vector-meson (VMD) like component, where the splitting is non-perturbative. The Monte Carlo models so far used assume the VMD-like topology for all events.

5 Summary

HERA data provides unique opportunities to study the structure and interactions of the photon. Jet production by both the whole photon and its parton constituents have been unambiguously observed, and jet cross sections are being used to test QCD and constrain the parton (particularly the gluon) distributions in the photon and the proton. Studies of the structure of the photon remnant give indications of a higher transverse remnant energy than is expected in simulations which describe the photon as a vector meson.

Acknowledgements

I am grateful to DESY and to KEK for assistance with travelling expenses, and to colleagues in the ZEUS and H1 collaborations for providing the material presented. This work was partially funded by the US National Science Foundation.

References

[1] H1 Collaboration, DESY 93-103.

[2] ZEUS Collaboration, The ZEUS detector, Status Report (1993) Available on WWW at http://zow00.desy.de:8000

[3] ZEUS Collaboration, M. Derrick et al., DESY 94-192, accepted for publication by Phys. Lett. B.

[4] R. Tanaka et al., AMY Collaboration Phys. Lett. B277 (1992) 215.

[5] H1 Collaboration, T. Ahmed et al., Phys. Lett. B297 (1992) 205.
ZEUS Collaboration, M. Derrick et al., Phys. Lett. B297 (1992) 404.

[6] ZEUS Collaboration, M. Derrick et al., Phys. Lett. B322 (1994) 287.

[7] H1 Collaboration, I. Abt et al., Phys. Lett. B314 (1993) 436.

[8] H1 Collaboration, I. Abt et al., Phys. Lett. B328 (1994) 176.

[9] ZEUS Collaboration, M. Derrick et al., Phys. Lett. B342 (1995) 417.

[10] J. Huth et al., Proc. of the 1990 DPF Summer Study on High Energy Physics, Snowmass, Colorado, edited by E.L. Berger (World Scientific, Singapore,1992) p. 134.
UA1 Collaboration., G. Arnison et al., Phys. Lett. 123B (1983) 115.

[11] H.-U. Bengtsson and T. Sjöstrand, Comp. Phys. Comm. 46 (1987) 43; T. Sjöstrand, CERN-TH.6488/92.

[12] G. Kramer and S.G. Salesch, Z. Phys. C61 (1994) 277;
L. E. Gordon and J. K. Storrow, Phys. Lett. B291 (1992) 320;
D. Bödeker, Z. Phys. C59 (1993) 501;
M. Greco and A. Vicini, Frascati preprint, LNF-93/017 (April 1993);
D. Bödeker, G. Kramer and S. G. Salesch, Z. Phys. C63 (1994) 471;
M. Klasen, G. Kramer and S. G. Salesch, DESY preprint DESY 94-232;
P. Aurenche et al., Phys. Lett. B338 (1994) 98.

[13] ZEUS Collaboration, M. Derrick et al., Phys. Lett. B348 (1995) 665.

[14] J. R. Forshaw and R. G. Roberts, Phys. Lett. B319 (1993) 539.

[15] M. Glück, E. Reya and A. Vogt, Phys. Rev. D46 (1992) 1973.

[16] W. Tung, Proc. of International Workshop on Deep Inelastic Scattering and Related Subjects, Eilat, Israel, 1994 World Sci., Singapore (to be published);
H. L. Lai et al., MSU-HEP-41024, CTEQ-404.

[17] A. Martin, W.J. Stirling and R.G. Roberts, Phys. Rev. D50 (1994) 6734.

[18] A. Martin, W.J. Stirling and R.G. Roberts, Phys. Rev. D47 (1993) 867.

[19] The CTEQ2 distributions use the final 1992 HERA data published in ZEUS Collab., M. Derrick et al., Phys. Lett. B316 (1993) 412; H1 Collab., I. Abt et al., Nucl. Phys. B407 (1993) 515.
MRSA uses the preliminary 1993 HERA data: ZEUS Collab., G. Wolf, Proc. of International Workshop on Deep Inelastic Scattering, Eilat, Israel, Feb. 1994; M. Roco, Proc. of 29th Rencontre de Moriond, March 1994 ; H1 Collab., K. Müller, *ibid.*

[20] J. R. Forshaw and R. G. Roberts, Phys. Lett. B335 (1994) 494.

[21] M. Drees and K. Grassie, Z. Phys. C28 (1985) 451.

[22] L. E. Gordon and J. K. Storrow, Z. Phys. C56 (1992) 307.

[23] H. Abramowicz, K. Charchula and A. Levy, Phys. Lett. B269 (1991) 458.

[24] G. Marchesini et al., Comp. Phys. Comm. 67 (1992) 465.

[25] G. A. Schüler and T. Sjöstrand, Nucl. Phys. B407 (1993) 539.
J. M. Butterworth and J. R. Forshaw, J. Phys. G19 (1993) 1657.
J. M. Butterworth and J. R. Forshaw, p.222 of the proceedings of the Workshop on Two-Photon Physics at LEP and HERA, Lund, May 26-28, 1994; Editors G. Jarlskog ans L. Jönsson.

[26] J. C. Collins and G. A. Ladinsky, Phys. Rev. D43 (1991) 2847.
J. R. Forshaw and J. K. Storrow, Phys. Lett. B268 (1991) 116; erratum B276.
R. S. Fletcher et al., Phys. Rev. D45 (1992) 337.

[27] Proceedings of the XXVII International Conference on High Energy Physics, Glasgow, Scotland, 20-27 July 1994, presented by H. Hufnagel.

[28] S. Catani, Yu. L. Dokshitzer, M. H. Seymour and B. R. Webber, Nucl. Phys. B406 (1993) 187.

[29] S. Catani, Yu. L. Dokshitzer and B. R. Webber, Phys. Lett. 285B (1992) 291.

[30] Proceedings of the XXVII International Conference on High Energy Physics, Glasgow, Scotland, 20-27 July 1994, presented by S. Bhadra.

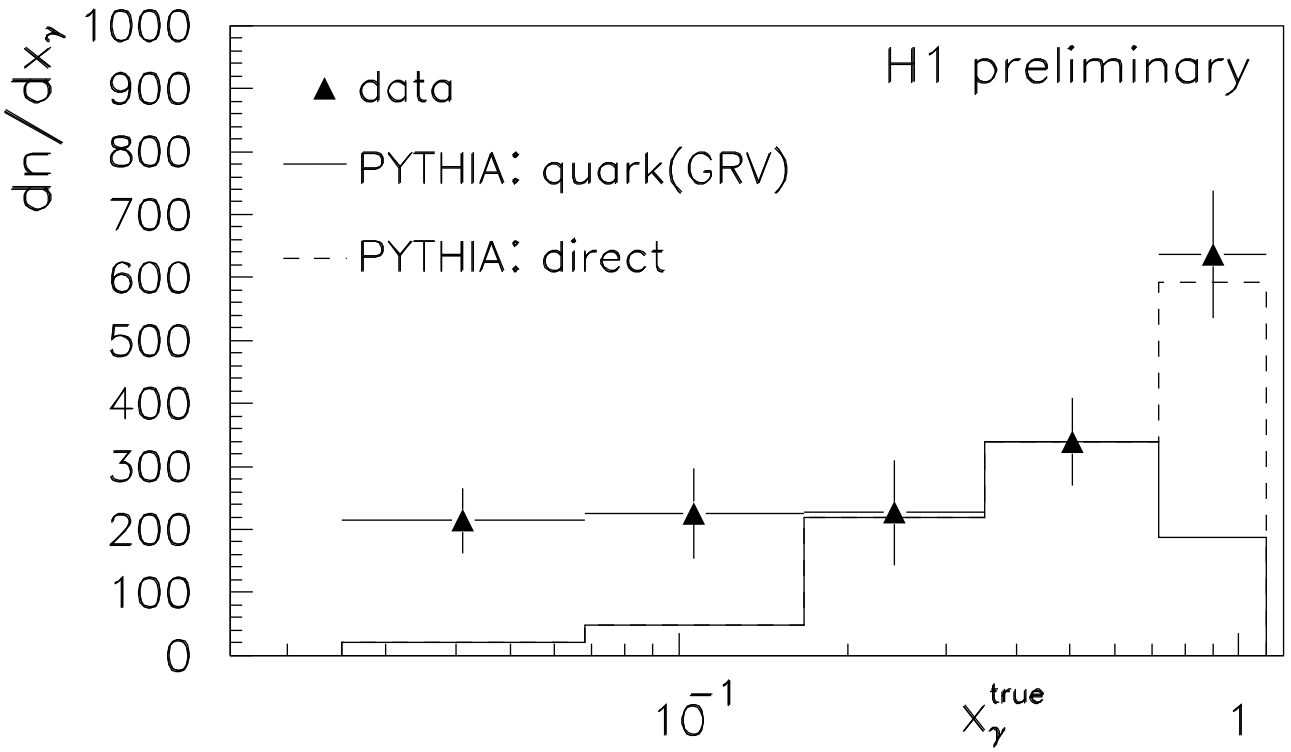

Figure 7: The x_γ^{LO} distribution unfolded using PYTHIA from events with two jets $E_T^{jet} > 7$ GeV and $\eta^{jet} < 2.5$.

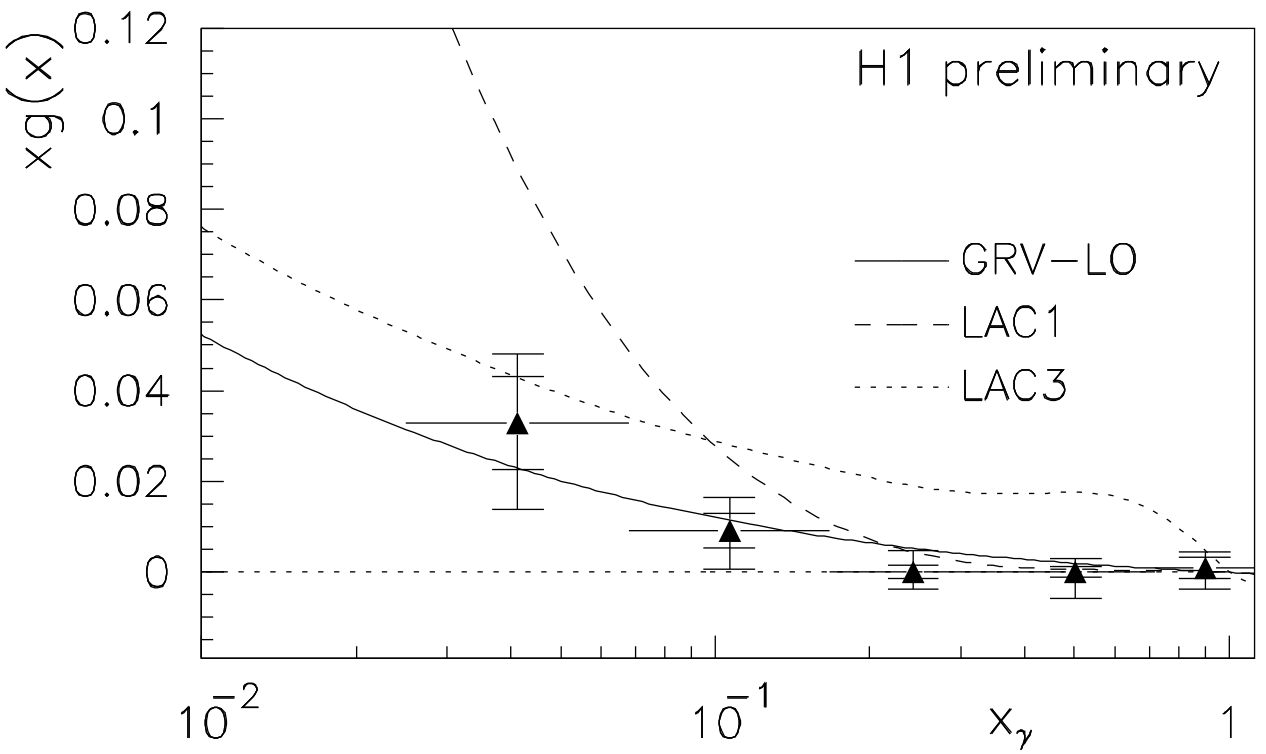

Figure 8: LO estimate of the gluon density in the photon unfolded using PYTHIA from events with two jets $E_T^{jet} > 7$ GeV and $\eta^{jet} < 2.5$.

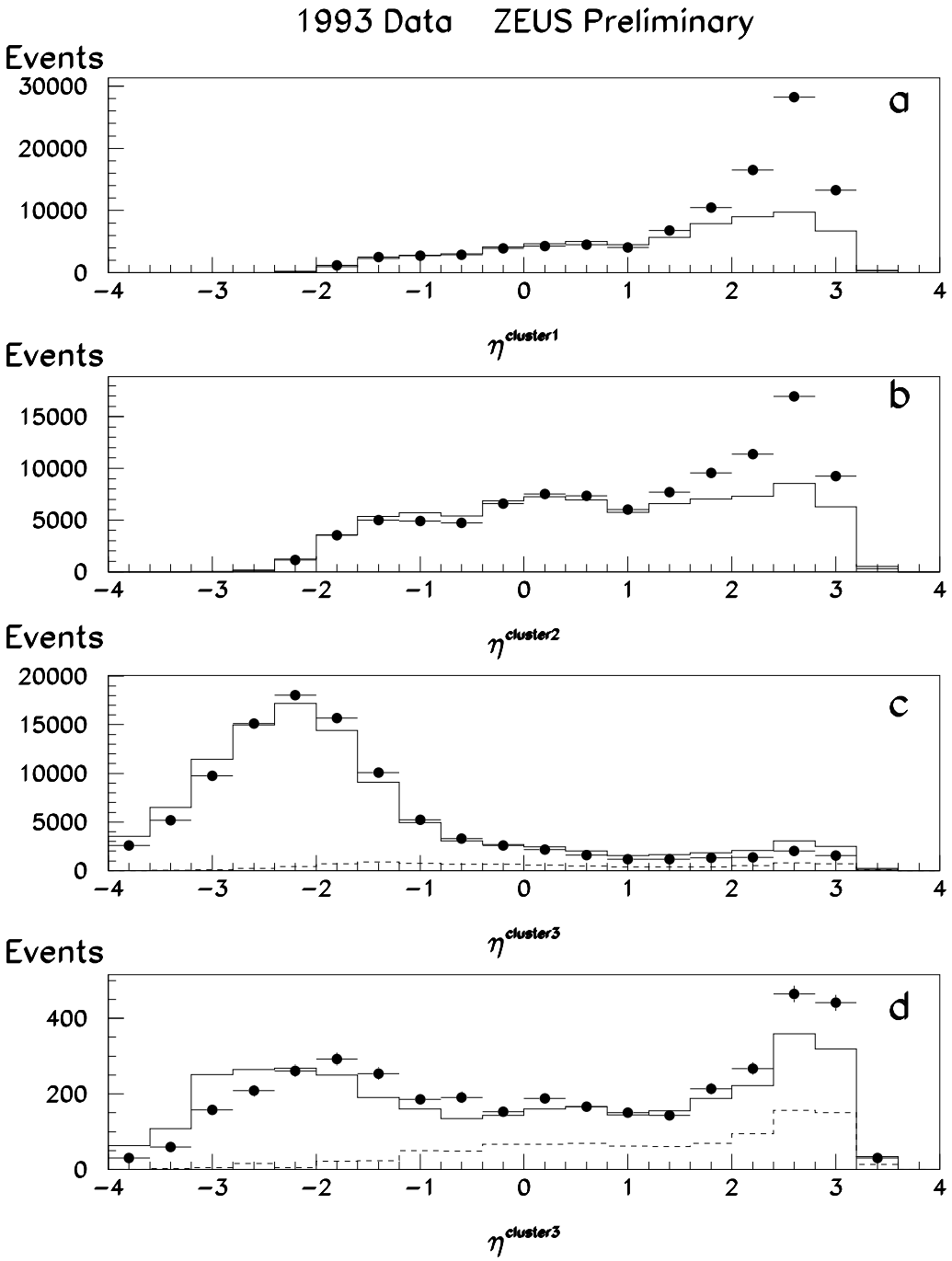

Figure 9: Pseudorapidity distributions of the first (a), second (b) and third (c) clusters found by the K_T algorithm: ZEUS data (full circles), MC direct+resolved (full histogram) and MC direct (dashed histogram). (d) as (c) but imposing a cut at $P_T^{cluster_{1,2}} \geq 5.0$ GeV and $\eta^{cluster_{1,2}} \leq 1.6$. Data and MC events are normalized in the region $\eta \leq 1.6$

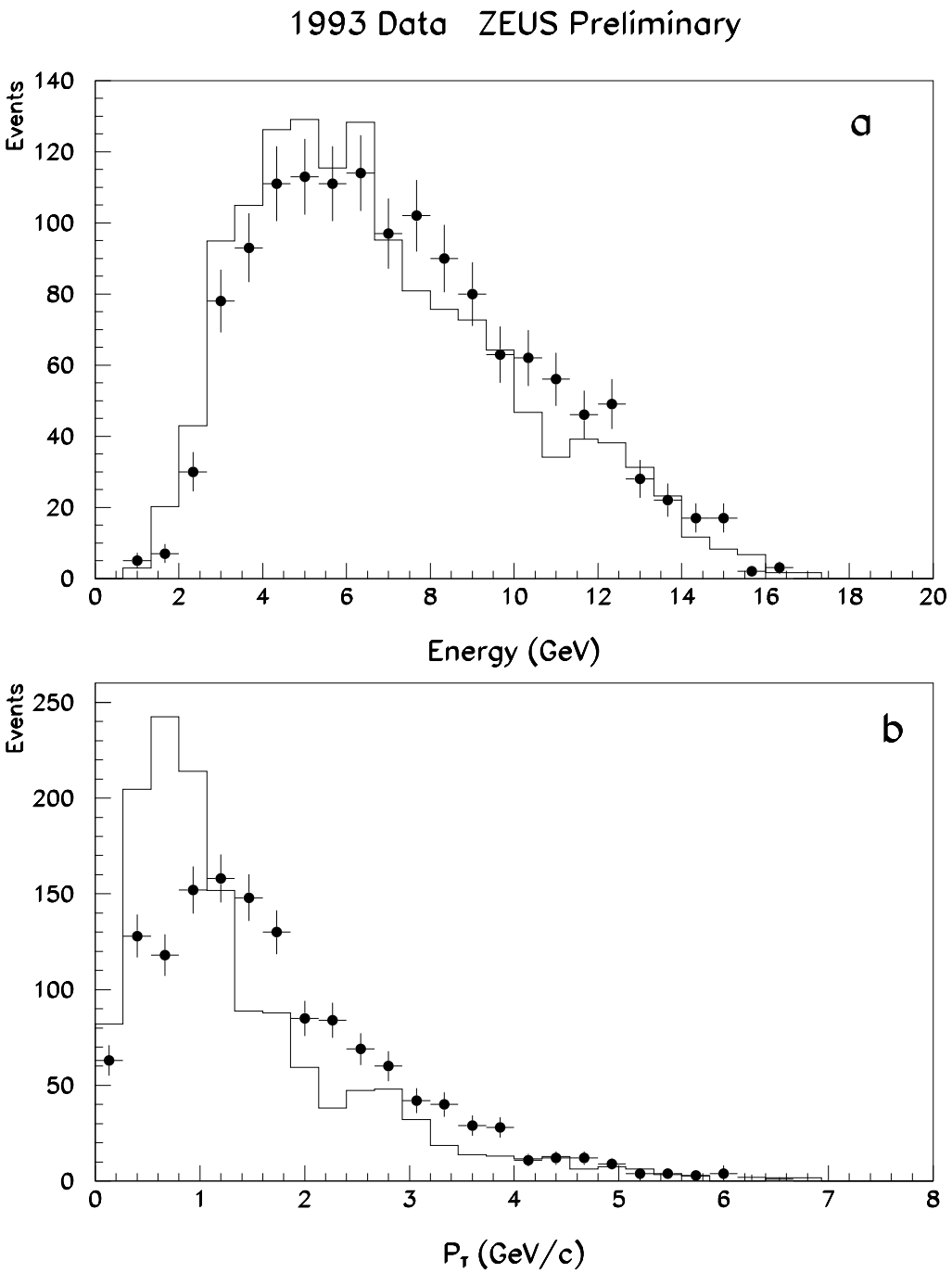

Figure 10: Energy (a) and $P_T^{cluster}$ (b) distributions for third cluster: ZEUS data (full circles) and MC direct+resolved (full histogram). Data and MC are normalized to the number of events in data.